



Calhoun: The NPS Institutional Archive

Theses and Dissertations

Thesis Collection

2001-03

Bandwidth optimization of underwater acoustic communications systems

Houdeshell, Jack E.

Monterey, California. Naval Postgraduate School

<http://hdl.handle.net/10945/2584>



Calhoun is a project of the Dudley Knox Library at NPS, furthering the precepts and goals of open government and government transparency. All information contained herein has been approved for release by the NPS Public Affairs Officer.

Dudley Knox Library / Naval Postgraduate School
411 Dyer Road / 1 University Circle
Monterey, California USA 93943

<http://www.nps.edu/library>

NAVAL POSTGRADUATE SCHOOL
Monterey, California



THESIS

**BANDWIDTH OPTIMIZATION OF UNDERWATER
ACOUSTIC COMMUNICATIONS SYSTEMS**

by

LT Jack E. Houdeshell

March 2001

Thesis Advisor:
Co-Advisor:

Kevin B Smith
Daniel T Nagle

Approved for public release; distribution is unlimited

20010618 087

REPORT DOCUMENTATION PAGE			Form Approved OMB No. 0704-0188	
Public reporting burden for this collection of information is estimated to average 1 hour per response, including the time for reviewing instruction, searching existing data sources, gathering and maintaining the data needed, and completing and reviewing the collection of information. Send comments regarding this burden estimate or any other aspect of this collection of information, including suggestions for reducing this burden, to Washington headquarters Services, Directorate for Information Operations and Reports, 1215 Jefferson Davis Highway, Suite 1204, Arlington, VA 22202-4302, and to the Office of Management and Budget, Paperwork Reduction Project (0704-0188) Washington DC 20503.				
1. AGENCY USE ONLY (Leave blank)	2. REPORT DATE March 2001	3. REPORT TYPE AND DATES COVERED Master's Thesis		
4. TITLE AND SUBTITLE: Title (Mix case letters) Bandwidth Optimization of Underwater Acoustic Communications Systems			5. FUNDING NUMBERS	
6. AUTHOR(S) Jack E. Houdeshell, LT. USN				
7. PERFORMING ORGANIZATION NAME(S) AND ADDRESS(ES) Naval Postgraduate School Monterey, CA 93943-5000			8. PERFORMING ORGANIZATION REPORT NUMBER	
9. SPONSORING / MONITORING AGENCY NAME(S) AND ADDRESS(ES) N/A			10. SPONSORING / MONITORING AGENCY REPORT NUMBER	
11. SUPPLEMENTARY NOTES The views expressed in this thesis are those of the author and do not reflect the official policy or position of the Department of Defense or the U.S. Government.				
12a. DISTRIBUTION / AVAILABILITY STATEMENT Approved for public release; distribution is unlimited			12b. DISTRIBUTION CODE	
13. ABSTRACT (maximum 200 words) Current underwater acoustic communication systems operate in the frequency band of 1 - 10 kHz and utilize various forms of signal processing to improve data rates. In this work, the influence of the environment on long-range propagation of acoustic signals will be examined over the band of 1-5 kHz. The transmission loss (TL) as a function of range over the bandwidth will be one measure to determine the optimal operating character of the communications channel. Additionally, estimates of signal variance over the bandwidth as a function of range will be computed. The variance will be generated from source platform motion and interface roughness. Particular attention will be paid to the 2 - 4 kHz band of certain operating systems for long-range transmission.				
14. SUBJECT TERMS : Underwater acoustic communication, bandwidth optimization, signal coherence.			15. NUMBER OF PAGES 58	
			16. PRICE CODE	
17. SECURITY CLASSIFICATION OF REPORT Unclassified	18. SECURITY CLASSIFICATION OF THIS PAGE Unclassified	19. SECURITY CLASSIFICATION OF ABSTRACT Unclassified	20. LIMITATION OF ABSTRACT UL	

NSN 7540-01-280-5500

Standard Form 298 (Rev. 2-89)
Prescribed by ANSI Std. Z39-18

THIS PAGE INTENTIONALLY LEFT BLANK

Approved for public release; distribution is unlimited

**BANDWIDTH OPTIMIZATION OF UNDERWATER ACOUSTIC
COMMUNICATIONS SYSTEMS**

Jack E. Houdeshell
Lieutenant, United States Navy
B.S., University of Idaho, 1994

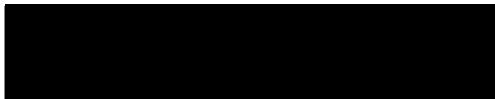
Submitted in partial fulfillment of the
requirements for the degree of

MASTER OF SCIENCE IN ENGINEERING ACOUSTICS

from the

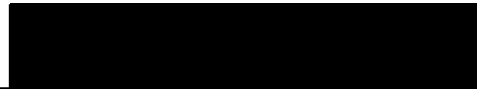
**NAVAL POSTGRADUATE SCHOOL
March 2001**

Author:



Jack E. Houdeshell

Approved by:



Kevin B. Smith, Thesis Advisor



Daniel T. Nagle, Co-Advisor



Kevin B. Smith, Chairman
Engineering Acoustics Academic Committee

THIS PAGE INTENTIONALLY LEFT BLANK

ABSTRACT

Current underwater acoustic communication systems operate in the frequency band of 1 - 10 kHz and utilize various forms of signal processing to improve data rates. In this work, the influence of the environment on long-range propagation of acoustic signals will be examined over the band of 1-5 kHz. The transmission loss (TL) as a function of range over the bandwidth will be one measure to determine the optimal operating character of the communications channel. Additionally, estimates of signal variance over the bandwidth as a function of range will be computed. The variance will be generated from source platform motion and interface roughness. Particular attention will be paid to the 2 - 4 kHz band of certain operating systems for long-range transmission.

THIS PAGE INTENTIONALLY LEFT BLANK

TABLE OF CONTENTS

I.	INTRODUCTION.....	1
II.	NUMERICAL METHODS	3
	A. MMPE MODEL	3
	1. Parabolic Equation Model.....	3
	2. MMPE and Doppler.....	8
	B. IMPLEMENTATION OF METHODS OF EVALUATION	12
	1. Transmission Loss.....	13
	2. Temporal Coherence.....	14
	3. Spatial Coherence.....	14
III.	DATA AND RESULTS.....	17
	A. ENVIROMENTAL DATA	17
	B. TRANSMISSION LOSS.....	18
	C. TEMPORAL COHERENCE.....	21
	D. SPATIAL COHERENCE.....	31
IV.	CONCLUSIONS	35
	A. CONCLUSIONS.....	35
	B. RECOMMENDATIONS FOR FURTHER RESEARCH	37
	LIST OF REFERENCES	39
	INITIAL DISTRIBUTION LIST	41

THIS PAGE INTENTIONALLY LEFT BLANK

LIST OF FIGURES

Figure 1: Geometry of source motion in the vertical plane along the radial between source and receiver.....	8
Figure 2: Sound velocity profiles used in MMPE model.....	17
Figure 3: Transmission loss versus frequency and range for SVP 1 with a flat bottom.	19
Figure 4: Transmission loss versus frequency and range for SVP 1 with a 2 m rms bottom roughness.	20
Figure 5: Transmission loss versus frequency and range for SVP 2 with a flat bottom.	20
Figure 6: Transmission loss versus frequency and range for SVP 2 with a 2 m rms bottom roughness.	21
Figure 7: Correlations for a source depth of 30 m and a receiver depth of 30 m comparing no Doppler and a roughness of 2 m to that of no Doppler and no roughness.....	23
Figure 8: Correlation for a source depth of 30 m and a receiver depth of 30 m comparing source speed of 5 m/s with no roughness to that of no Doppler and no roughness.....	23
Figure 9: Correlation for a source depth of 30 m and a receiver depth of 30 m comparing source speed of 5 m/s with a roughness of 2 m to that of no Doppler and no roughness.....	24
Figure 10: Maximum value of the cross-correlation for each center frequency with a roughness of 2 m and zero speed for (a, c, e) and a roughness of 2 m and speed of 5 m/s for (b, d, f). The data was calculated using SVP 1, a source depth of 30 m and receiver depths of (a, b) 30 m, (c, d) 50 m, and (e, f) 70 m.....	25
Figure 11: Maximum value of the cross-correlation for each center frequency with a roughness of 2 m and zero speed for (a, c, e) and a roughness of 2 m and speed of 5 m/s for (b, d, f). The data was calculated using SVP 1, a source depth of 50 m and receiver depths of (a, b) 30 m, (c, d) 50 m, and (e, f) 70 m.....	26
Figure 12: Maximum value of the cross-correlation for each center frequency with a roughness of 2 m and zero speed for (a, c, e) and a roughness of 2 m and speed of 5 m/s for (b, d, f). The data was calculated using SVP 1, a source depth of 70 m and receiver depths of (a, b) 30 m, (c, d) 50 m, and (e, f) 70 m.....	27
Figure 13: Maximum value of the cross-correlation for each center frequency with no roughness and a source speed of 5 m/s and for a receiver depth of (a) 30 m,(b) 50 m, and (c) 70 m for SVP 1 and a source depth of 50 m.	28
Figure 14: Maximum value of the cross-correlation for center frequency of 2 and 4 kHz with a rms bottom roughness of 2 m, a source and receiver depth of 30 m, and (a,b) bottom shift with no source speed, (c,d) bottom shift and source speed of 5 m/s, and (e,f) no bottom shift and source speed of 5 m/s for SVP 1 (a,c,e) and SVP 2 (b,d,f).....	30

Figure 15: Plot of the maximum correlation for each frequency at each range for SVP 1 using no source speed and rms roughness of 2 m with source depth of 30 m.....	31
Figure 16: Plot of maximum correlation for source depths 30 m (a, b), 50 m (c, d), and 70 m (e, f) with (a, c), and (e) using no speed with roughness of 2 m and (b, d, f) using a speed of 5 m/s and roughness of zero.....	33
Figure 17: Plot of the maximum correlation for each frequency at each range for SVP 1 using the shifted bottom with no source speed and rms roughness of 2 m with source depth of 50 m.....	34
Figure 18: Plot of the maximum correlation for each frequency at each range for SVP 2 using the shifted bottom with no source speed and rms roughness of 2 m with source depth of 50 m.....	34

ACKNOWLEDGMENTS

As with any project that cumulates two years of work, there are many people to thank.

For me, three of the most important are Diane, my wife, Jordan and Alexa, my daughters. They provided me the support and motivation to keep me going.

My thesis advisor, Professor Kevin Smith, has given much of his time and effort in making my thesis a success. His knowledge of signal processing as well as acoustics was invaluable to the completion of my thesis.

Dr. Daniel Nagle from Naval Undersea Warfare Center, Keyport provided guidance in directing me where I should focus my thesis. He also supported my thesis by being my co-advisor.

The numbers of others are too numerous to mention their contribution but they include:

CDR. Jim Hill, Code 35 Curric Officer

Eva Anderson, Code 35 Educational Specialist

Physics Department Faculty and Staff

My fellow students in the Engineering Acoustics pipeline

THIS PAGE INTENTIONALLY LEFT BLANK

I. INTRODUCTION

Reflecting the changing times, the United States Navy has emerged with a new doctrine, *Forward From the Sea*. With this new doctrine, the Navy is moving from the blue water in which it has been accustomed into the grey water, or littoral, in which it has not. Submarines play a vital role supporting the new doctrine. Many of the requirements demand that the submarine remain in contact with the battlegroup, deploy unmanned vehicles, and perform peacetime surveillance and reconnaissance all while the submarine maintains its depth and speed (Curtin and Benson, 1999). In order to maintain continuity with these groups, a reliable communication channel needs to be available.

Electromagnetic channels would at first seem to be the ideal method for communication since it is already established as the primary means of communication for surface ships. But electromagnetic radiation (light, radio waves, lasers, etc.) does not penetrate seawater to any great distances. Even the blue-green laser only penetrates seawater to a distance of less than 100 m. Most underwater communication systems need to be able to communicate over several kilometers to hundreds of kilometers. The only channel available for these distances is the underwater acoustic, often referred to as acoustic communications (or AComms), channel (Curtin and Benson, 1999).

There are many factors affecting the use of the AComms channel: transmission loss (TL), temporal coherence, and spatial coherence. These factors are affected by the varying ocean environment and the operating frequency. Such things as ducting, bottom losses and reflection, and surface reflection affect TL. Further, variations in the temporal and spatial coherence are areas that still need to be studied to fully understand their influence (Kilfoyle and Baggeroer, 2000).

The aim of this thesis is to analyze the AComms channel and evaluate the optimal center frequency between 1 and 5 kHz using a 2 kHz bandwidth. This evaluation will encompass two sound velocity profiles (SVPs), varying source and receiver depths, and varying bottom roughness. In order to perform this evaluation, the Monterey-Miami Parabolic Equation (MMPE) model is employed. From the data provided, three methods of evaluation (MOE) will be utilized to optimize the center frequency: transmission loss, temporal coherence, and spatial coherence.

The organization of this thesis will take the following format. Chapter II will discuss the MMPE model and the MOE's employed. Chapter III will present the data acquired and the trends observed. Finally, Chapter IV will discuss the conclusions and future work that is needed.

II. NUMERICAL METHODS

This chapter presents an overview of the MMPE model utilized for this thesis. The MOE's will also be defined.

A. MMPE MODEL

1. Parabolic Equation Model

The parabolic equation (PE) method has become the preferred method of solving the underwater acoustic range-dependent problem. The MMPE Model is based upon the parabolic approximation of the wave equation and thus a brief description of this approach is useful.

For this discussion we will start with the linearized wave equation provided below in Eq. (2.1). Next, if there is a continuous wave source, the pressure field can be described by the product of a pressure amplitude, dependent on the position, and a time varying exponential (Jensen, et al., 2000):

$$\nabla^2 P + \frac{1}{c^2} \frac{\partial^2 P}{\partial t^2} = 0, \quad (2.1)$$

$$P(\bar{x}, t) = p(\bar{x})e^{-i\omega t}. \quad (2.2)$$

Substituting Eq. (2.2) into Eq. (2.1), the Helmholtz equation can be derived (Jensen, et al., 2000),

$$\nabla^2 p(\bar{x}) - \frac{\omega^2}{c^2} p(\bar{x}) = 0. \quad (2.3)$$

The ocean acts as a very thin waveguide on the surface of the planet, and so a cylindrical coordinate system is the natural choice, i.e. $p(r, z, \phi)$. The ocean environment,

and thus the underwater acoustic field, tends to exhibit only weak azimuthal dependence.

This allows us to ignore the azimuthal terms, and define the complex acoustic pressure

$$P(r, z, \omega t) = p(r, z)e^{-i\omega t}. \quad (2.4)$$

Let's assume the pressure field can be defined by (Smith and Tappert, 1993)

$$p(r, z) = \frac{1}{\sqrt{r}}u(r, z). \quad (2.5)$$

The $1/\sqrt{r}$ term accounts for the azimuthal spreading and $u(r, z)$ is the two-dimensional pressure field. Substituting Eqs. (2.4) and (2.5) into Eq. (2.3) yields (Smith, 2001a)

$$\frac{\partial^2 u}{\partial r^2} + \frac{\partial^2 u}{\partial z^2} + k_o^2 \left(n^2 + \frac{1}{4k_o^2 r^2} \right) u = 0. \quad (2.6)$$

This is referred to as the uncoupled azimuth approximation since the azimuthal variations have been ignored. If we now introduce the operator notation

$$P_{op} = \frac{\partial}{\partial r} \quad (2.7)$$

and

$$Q_{op} = (\mu + \varepsilon + 1)^{\frac{1}{2}} \quad (2.8)$$

where

$$\varepsilon = n^2 - 1 \text{ and } \mu = \frac{1}{k_o^2} \frac{\partial^2}{\partial z^2}, \quad (2.9)$$

we may rewrite Eq. (2.6) using the operators defined above as

$$(P_{op}^2 + k_o^2 Q_{op}^2) u = 0. \quad (2.10)$$

If we further define

$$u = Q_{op}^{-1/2} \Psi, \quad (2.11)$$

then the outgoing wave must satisfy (Smith, 2001a)

$$-ik_0^{-1} \frac{\partial \Psi}{\partial r} = Q_{op} \Psi. \quad (2.12)$$

Eq. (2.12) is the foundation for all PE models. What separates different models is the method of generating solutions to this equation and the approximations of the operator Q_{op} .

To develop a numeric algorithm, it is useful to decompose the field into a slowly modulating envelope function and a rapidly varying phase term. The envelope function, or field function $\psi(r, z)$, is defined by (Smith, 2001a)

$$\Psi = \psi e^{ik_0 r} \quad (2.13)$$

or, in terms of acoustic pressure,

$$p(r, z) = P_o \sqrt{\frac{R_o}{r}} Q_{op}^{-1/2} \psi(r, z) e^{ik_0 r}. \quad (2.14)$$

The parabolic equation for the field function is then defined by (Smith, 2001a)

$$\frac{\partial \psi}{\partial r} = -ik_0 \psi + ik_0 Q_{op} \psi = -ik H_{op} \psi, \quad (2.15)$$

where

$$H_{op} = 1 - Q_{op} \quad (2.16)$$

is a Hamiltonian-like operator, which defines the evolution of the PE field function in range.

The relationship between values of ψ at different ranges can be defined by (Smith, 2001a)

$$\psi(r + \Delta r) = \Phi(r)\psi(r), \quad (2.17)$$

where $\Phi(r)$ is a unitary operator that marches the solution out in range. The MMPE model employs a split-step Fourier (PE/SSF) method to provide a representation of the propagator $\Phi(r)$. This method is utilized primarily based on the speed and simplicity of the PE/SSF.

The H_{op} operator must be separated which requires an approximation to the square root operator. The approximation of the Hamiltonian operator used in the MMPE corresponds to the so-called wide-angle PE (WAPE) approximation (Thomson and Chapman, 1983):

$$H_{op} \approx T_{op} + U_{op}, \quad (2.18)$$

where

$$T_{op}(k) = 1 - \left[1 + \frac{1}{2k_0^2} \frac{\partial^2}{\partial z^2} \right]^{\frac{1}{2}} \quad (2.19)$$

and

$$U_{op} = -[n - 1]. \quad (2.20)$$

The propagation function $\Phi(r)$ can then be shown to take the form (Smith, 2001a)

$$\Phi(r) = e^{-ik_o \frac{\Delta r}{2} U_{op}(r+\Delta r)} e^{-ik_o \Delta r T_{op}} e^{-ik_o \frac{\Delta r}{2} U_{op}(r)} \quad (2.21)$$

To simplify the calculations, the PE/SSF algorithm employs the operator $e^{-ik_o \Delta r \hat{T}_{op}}$ in the k_z -domain where

$$\hat{T}_{op} = 1 - \left[1 - \left(\frac{k_z}{k_o} \right)^2 \right]^{1/2} \quad (2.22)$$

With the fast Fourier transform employing the convention

$$\psi(z) = FFT(\psi(k_z)) \quad (2.23)$$

and

$$\psi(k_z) = IFFT(\psi(z)), \quad (2.24)$$

the PE/SSF implementation can be represented by (Smith, 2001a)

$$\psi(z, r + \Delta r) = e^{-ik_o \frac{\Delta r}{2} U_{op}(z, r + \Delta r)} \times FFT \left\{ e^{-ik_o \Delta r \hat{T}_{op}(k_z)} \times IFFT \left(e^{-ik_o \frac{\Delta r}{2} U_{op}(z, r)} \times \psi(z, r) \right) \right\} \quad (2.25)$$

Bottom roughness and its effect on scattering of the pressure field have been included in this version of the MMPE Model used in this thesis. Li (2000) described a method for computing the mean squared reverberation from different roughness realizations. In his work it was necessary to define statistical realizations of bottom roughness. This realization was implemented using a power spectrum defined by (Li, 2000)

$$W(K) = (1 + L_{corr}^2 K^2)^{-\left(\frac{\beta_n}{2}\right) + \left(\frac{1}{2}\right)}, \quad (2.26)$$

where L_{corr} is the correlation length, β_n is the spectral exponent, and K is the horizontal wavenumber in the radial direction.

2. MMPE and Doppler

Source/receiver motion causes temporal fluctuations and modeling these changes is important to understanding the acoustic underwater channel for such applications as communications (Kilfoyle and Baggeroer, 2000). Figure 1 shows the geometry of the Doppler problem caused by source motion. This motion causes the actual source frequency observed, $f_s(\theta)$, to become a function of the transmitted frequency, f_T , the observation angle, θ , the source speed, v_s , and the direction of motion, ϕ_s (Smith, 2001b),

$$f_s(\theta) = \frac{f_T}{1 - (v_s/c)\cos(\theta - \phi_s)} \approx f_T [1 + (v_s/c)\cos(\theta - \phi_s)]. \quad (2.27)$$

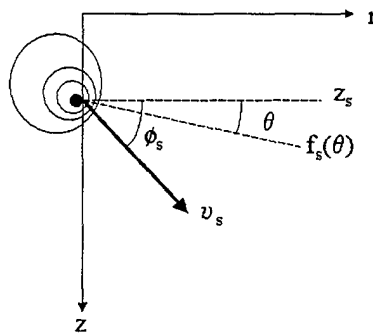


Figure 1: Geometry of source motion in the vertical plane along the radial between source and receiver

It can be shown that for $|\phi_s| < 90^\circ$ the observed frequency bandwidth downrange, BW_s^{r+} becomes (Smith, 2001b)

$$BW_s^{r+} = BW_T + \frac{v_s}{c} (f_{T,\max} + f_{T,\min} |\sin \phi_s|), \quad (2.28)$$

where BW_T is the actual transmitted bandwidth, $f_{T,\max}$ and $f_{T,\min}$ are the actual transmitted maximum and minimum frequencies, respectively, of the transmitted band, and the observed center frequency downrange is (Smith, 2001b)

$$f_{s,c}^{r+} = f_{T,c} + \frac{v_s}{2c} (f_{T,\max} - f_{T,\min} |\sin \phi_s|), \quad (2.29)$$

where $f_{T,c}$ is the actual transmitted center frequency. If $|\phi_s| > 90^\circ$, the observed bandwidth downrange becomes (Smith, 2001b)

$$BW_s^{r-} = BW_T + \frac{v_s}{c} (f_{T,\max} |\sin \phi_s| + f_{T,\min}), \quad (2.30)$$

and the observed center frequency becomes

$$f_{s,c}^{r-} = f_{T,c} + \frac{v_s}{c} (f_{T,\max} |\sin \phi_s| + f_{T,\min}). \quad (2.31)$$

The general form for the PE starting field in the vertical wavenumber domain may be written (Smith, 2001b)

$$\hat{\psi}(r=0, k_z, f) = e^{-ik_z z_s} \hat{\psi}_o(k_z, f) - e^{ik_z z_s} \hat{\psi}_o(k_z, f), \quad (2.32)$$

where the functions $\hat{\psi}_o(k_z, f)$ represent the starting field in free space and the influence of the exponentials is to produce the proper interference structure between the source at

depth z_s and its image about the free surface at depth $z=0$. In terms of the horizontal angle of propagation and the acoustic parameters, the vertical wavenumber is defined by

$$k_z = k_o \sin \theta = \frac{2\pi f}{c_o} \sin \theta. \quad (2.33)$$

For this thesis, a point source is modeled such that (Smith, 2001b)

$$\hat{\psi}_o(k_z, f) = \alpha(k_o)S(f), \quad (2.34)$$

where

$$\alpha(k_o) = \sqrt{\frac{iR_o}{2\pi k_o}}, \quad (2.35)$$

and $S(f)$ is the amplitude spectrum of the pulse in the frequency domain. The MMPE implementation uses a Hanning window to define this spectrum,

$$S(f) = \begin{cases} \cos^2\left(\frac{f - f_c}{BW} \pi\right), & |f - f_c| < BW/2, \\ 0, & |f - f_c| > BW/2 \end{cases}, \quad (2.36)$$

where f_c is the center frequency of the transmitted band and BW is the transmission bandwidth.

For a moving source, Eq. (2.32) must be rewritten in terms of the transmission parameters (Smith, 2001b),

$$\hat{\psi}(r=0, k_z, f) = e^{-ik_z z_s} \hat{\psi}_o(k_{z,T}, f_T) - e^{ik_z z_s} \hat{\psi}_o(k_{z,T}, f_T), \quad (2.37)$$

where

$$k_{z,T} = \frac{k_o \sin \theta}{\left[1 + \frac{v_s}{c_o} \cos(\theta - \phi_s) \right]} \quad (2.38)$$

and the frequency in the environmental reference frame was created by the source transmitting at f_T with the relationship between the two frequencies given by Eq. (2.27). Note that now the source spectrum $S(f)$ in Eq. (2.36) is replaced by (Smith, 2001b)

$$S(f_T) = S \left(\frac{f}{\left[1 + \frac{v_s}{c_o} \cos(\theta - \phi_s) \right]} \right). \quad (2.39)$$

This source spectrum must be applied to the starting field prior to the calculations and cannot be applied to the results in the post-processing. Additionally, the factor α must be replaced by the corresponding transmitted value α_T .

To allow comparison between the cases with and without Doppler, the frequency window of the non-Doppler case had to be adjusted to be the same size as the Doppler case. For the non-Doppler case, the frequency window is determined similarly to the Doppler case, except a weighting of zero is applied to those frequency bins that are outside of the non-Doppler bandwidth.

B. IMPLEMENTATION OF METHODS OF EVALUATION

The ocean environment is not constant. Because of that, motion of the ocean can easily cause the ship to roll and yaw. This motion, in turn, causes some of the parameters of the acoustic channel to vary, such as position relative to bottom roughness, speed in the direction of transmission, or a combination of the two. These variations can cause the multipath arrival structure of the signal to change, producing degradations in temporal and spatial coherence and even affecting TL levels. The received multipath will impact cross-correlation estimates due to frequency-selective interference of each arrival and the number of arrivals. In addition, the effects of Doppler shifts of the spectrum are anticipated to reduce the cross-correlation. Note that equalization signal processing techniques have been investigated to combat effects of multipath and Doppler (Stojanovic, et al., 1993). Thus, the coherence measurement results highlight the severity of these effects for different environments and infer the benefits of signal processing to compensate these effects.

An evolving rough surface can also affect results but will not be modeled here. Such effects may be expected to be similar to rough bottom effects. Direct investigations into the effects of a rough surface will be left to future work.

To numerically evaluate the changes introduced by such perturbations, the MMPE model was used to generate a pressure signal for four sets of conditions: stationary source and smooth bottom, stationary source and 2 m rms bottom roughness, 5 m/s source speed and smooth bottom, and finally 5 m/s source speed and 2 m rms bottom roughness. The AComms channel is, therefore, very complex. Thus, only three simple

MOE's will be employed: transmission loss (TL), temporal coherence, and spatial coherence.

1. Transmission Loss

Transmission loss has been studied for many years and is included in this thesis as a fundamental measure. There is a direct correlation between the source power required and TL. For a passive receiver in an AComms system to detect the incoming signal, the source level must satisfy (Kinsler, et al., 2000)

$$SL - TL \geq NL - DI + DT, \quad (2.40)$$

where NL is the noise level over the band of interest, DI is the receiver directivity index, and DT refers to a detection threshold used to define acceptable levels of reception. In the frequency band of interest, the right hand side of this equation is essentially constant. Thus, we could simplify the equation in this case to

$$SL \geq TL + C, \quad (2.41)$$

where C is a constant. Because the source level is directly related to the source power output, higher levels of TL require more power. Frequency bands of low TL would, therefore, optimize the power requirements of the system.

The evaluation of TL will be based on data computed with both a flat bottom and a rough bottom interface with 2 m rms roughness. Since we are evaluating TL as a function of frequency, no Doppler will be analyzed. Furthermore, we will only consider a source and receiver depth of 50 m. In terms of the field function ψ , TL will be calculated according to

$$TL = -20 \log \left(\frac{|p|}{p_o} \right) = -20 \log(|\psi|) + 10 \log \left(\frac{r}{R_o} \right), \quad (2.42)$$

where R_o is a reference range of 1 m.

2. Temporal Coherence

From each set of parameters and a set range and depth, the pressure signal as a function of frequency, $p_{r,z}(f)$, was extracted from the model data. An inverse fast Fourier transform was used to transform the pressure signal into the time domain:

$$p_{r,z}(t) = IFFT(p_{r,z}(f)). \quad (2.43)$$

Next, the pressure fields were cross-correlated over time at a fixed source and receiver depth using the stationary source and smooth bottom data as the reference. This can be written as (Proakis and Manolakis, 1996):

$$r_{pp'}(\delta_i) = \sum_t p_{r,z}(t) p_{r,z}'(t - \delta_i) / \max(r_{pp}), \quad (2.44)$$

where $p_{r,z}(t)$ is the reference signal in the time domain, $p_{r,z}'(t)$ is the pressure signal in the time domain, $r_{pp'}$ is the cross-correlation sequence normalized by the auto-correlation of the reference pressure signal, r_{pp} , and δ_i is the time shift. Of particular interest will be the peak value of the cross-correlation.

3. Spatial Coherence

To evaluate the spatial variations, the pressure field was extracted for a given range over the entire depth for each frequency, $p_{r,f}(z)$. The pressure field is then cross-correlated over depth using the stationary source and smooth bottom data as a reference for various source depths (Proakis and Manolakis, 1996):

$$r_{pp'}(\delta_z) = \sum_z p_{r,f}(z) p_{r,f}'(z - \delta_z) / \max(r_{pp}), \quad (2.45)$$

where $p_{r,f}(z)$ is the reference signal for the given frequency, $p_{r,f}'(z)$ is the pressure signal for the given frequency, $r_{pp'}$ is the cross-correlation sequence normalized by the auto-correlation of the reference pressure signal, and δ_z is the spatial shift. As before, the peak value of the cross-correlation will be of particular interest in the analysis.

THIS PAGE INTENTIONALLY LEFT BLANK

III. DATA AND RESULTS

A. ENVIROMENTAL DATA

For this thesis, two sound velocity profiles (SVP) were considered. The first was from the continental shelf off the United States East Coast. It actually extended down to 350 m, but for the work in this thesis it was truncated at 100 m. The second SVP was from the Pacific Ocean off the Southern California coast. This SVP was to a water depth of 100 m. Both are graphed in Figure 2. The bottom characteristics used for both SVP's were the same. A 1600 m/s sound speed with a gradient of 1 s^{-1} , 1.2 density ratio to water, and 0.1 dB/m/kHz absorption coefficient were used.

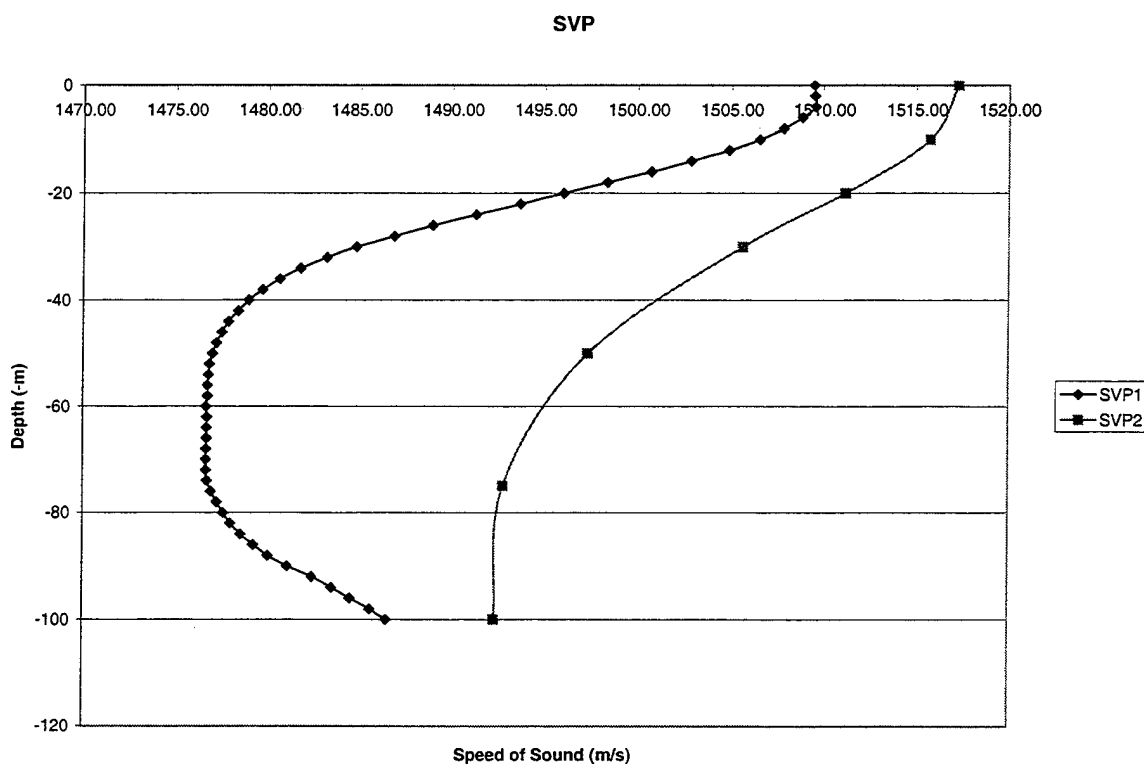


Figure 2: Sound velocity profiles used in MMPE model.

B. TRANSMISSION LOSS

Normally the frequency domain response is weighted with a Hanning window to represent a simple pulse. To find the optimum frequency it was necessary to have all frequencies weighted equally. Therefore a square window was applied to the frequency envelope. The frequency ranged from 200 Hz to 5 kHz using 200 Hz frequency bandwidths. Source and receiver depths were both selected to be 50 m. The above parameters were selected to cover the frequency range of interest and to compare with the results presented in previous work by others (Jensen and Kuperman, 1983). For comparison, the TL calculated from the MMPE model was smoothed to remove the fine-scale details and was then plotted as a function of frequency and range. Because Doppler effects are not expected to significantly affect this part of the analysis, the only variations considered here are the structure of the SVP and the bottom roughness. The TL data for SVP 1 without and with a rough bottom are presented in Figures 3 and 4, respectively. The corresponding plots for SVP 2 are presented in Figures 5 and 6.

In Figure 3, the TL is essentially constant for all frequencies at any given range. Similarly, Figure 5 doesn't show any relationship between frequency and TL as a function of range. The TL in Figure 4 is greater than in Figure 3, but at ranges greater than 20 km there is a weak relationship between frequency and range. Greater TL in Figure 4 than in Figure 3 is due to the increased scattering at short range from the increase in bottom roughness. The apparent frequency dependence at long range is due to limited, but continual bottom interactions at the bottom of the SVP 1 sound channel. Figure 6 shows an even stronger relationship for all ranges. In both Figures 4 and 6, the TL increases with increasing frequencies. Data from Jensen and Kuperman is very

similar to Figure 6 which shows a distinctive optimal frequency within the band. It appears that two factors are required to develop such a relationship between frequency and TL. The first is a strong bottom interaction. SVP 1 has a sound channel that would minimize interaction with the bottom, reducing the influence of bottom interactions and frequency dependence, whereas SVP 2 has a negative gradient all the way to the bottom causing strong interaction with the bottom. Secondly, it appears that a rough bottom, or some other form of additional reflection loss, is necessary. A flat bottom produces specular reflections with little bottom loss for all angles of interaction. A sufficiently rough bottom introduces scattering into angles steeper than critical, causing bottom penetration and enhanced bottom loss. This effect is more pronounced at higher frequencies. Similarly for the case studied by Jensen and Kuperman, a shear-supporting bottom was needed to account for the additional bottom loss.

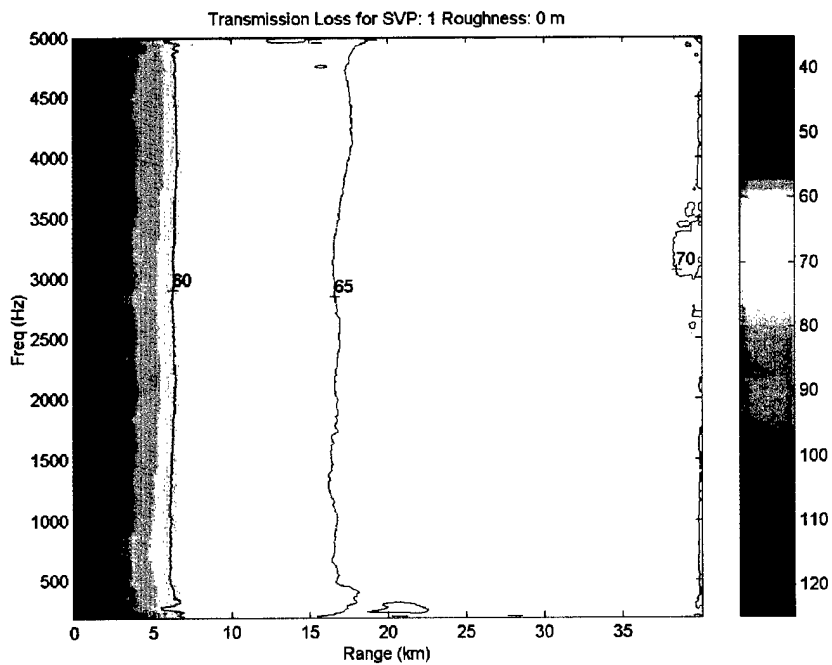


Figure 3: Transmission loss versus frequency and range for SVP 1 with a flat bottom.

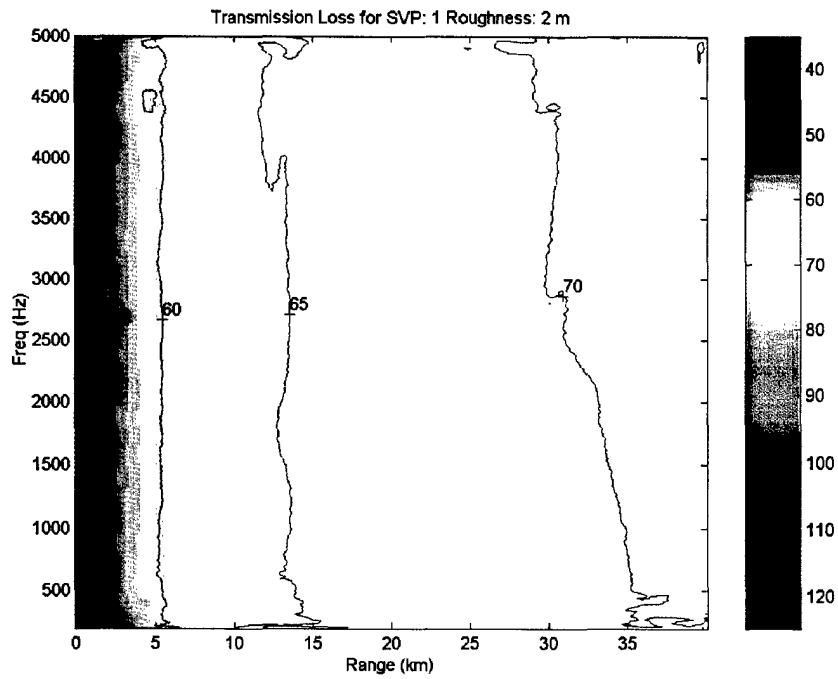


Figure 4: Transmission loss versus frequency and range for SVP 1 with a 2 m rms bottom roughness.

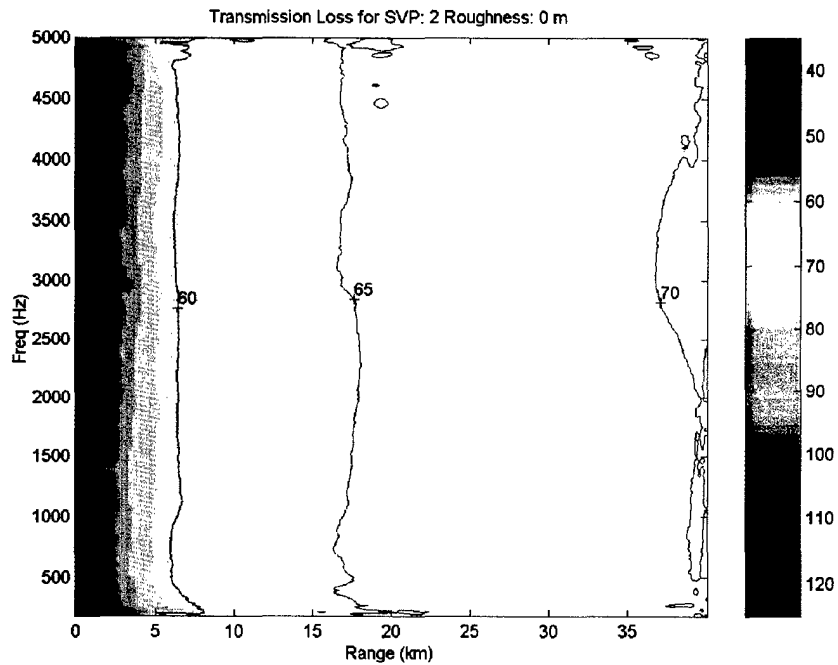


Figure 5: Transmission loss versus frequency and range for SVP 2 with a flat bottom.

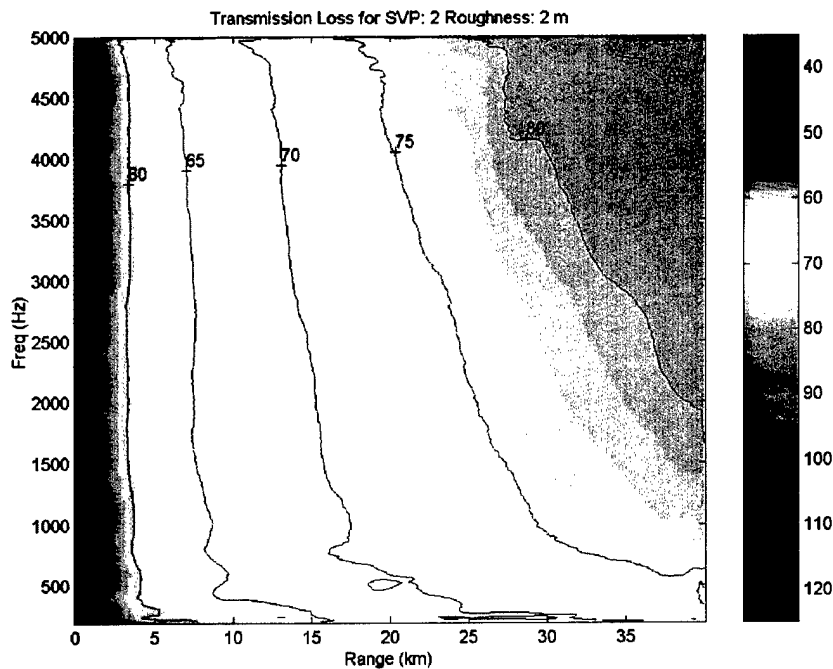


Figure 6: Transmission loss versus frequency and range for SVP 2 with a 2 m rms bottom roughness.

C. TEMPORAL COHERENCE

To examine the signal coherence in the time domain for the different perturbations, three frequency bands were considered centered at 2, 3, and 4 kHz each with a 2 kHz bandwidth. To obtain adequate sampling, 2048 frequencies were used across the bandwidth for the MMPE model. Three source depths (30, 50, and 70 m) were also used. This generated 12 data files for each of the center frequencies for each SVP. The data files stored 100 points in range and 64 points in depth with 32 of the depth points in the water column. Five ranges and three receiver depths were selected from the data set. The five ranges were 2.02, 4.04, 6.06, 8.08, and 10 km, and the three receiver depths were approximately 30, 50, and 70 m. To keep track of the various combinations

in the files, a naming convention was adopted. An example name is cf2sd30rd50sp5r2, where

cf-center frequency in kHz

sd-source depth in meters

rd-receiver depth in meters

sp-source speed in m/s

r -bottom roughness in m

Figures 7, 8, and 9 are graphs of the time domain signal correlations for SVP 1 with a source and receiver depth of 30 m and a range of 2.02 km. These graphs are a representative sample of the outcome of the correlations when source motion-induced Doppler and bottom roughness are added. The graphs show a strong correlation in the presence of Doppler when the bottom was smooth. This is perhaps not surprising since 5 m/s is not a large change compared to the sound speed (approximately 1500 m/s). The bottom roughness of 2 m rms, on the other hand, has a significant effect on the cross-correlation of the signal with the result obtained using no roughness. If a threshold of .5 were used to distinguish between correlated and uncorrelated, the bottom roughness generally caused the signal to be completely uncorrelated. On Figures 7 and 9, the vertical dashed lines mark the position of the maximum peak in the cross-correlation while the horizontal dashed lines mark the amplitude of the maximum peak of the cross-correlation. These lines are not visible in Figure 8 since its peak is at zero and is almost unity and so is masked by the index lines.

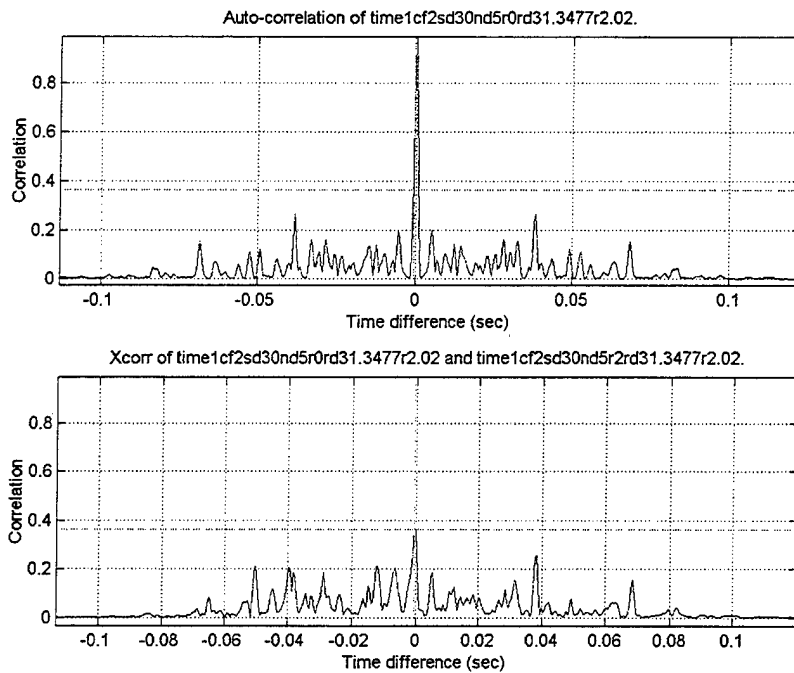


Figure 7: Correlations for a source depth of 30 m and a receiver depth of 30 m comparing no Doppler and a roughness of 2 m to that of no Doppler and no roughness.

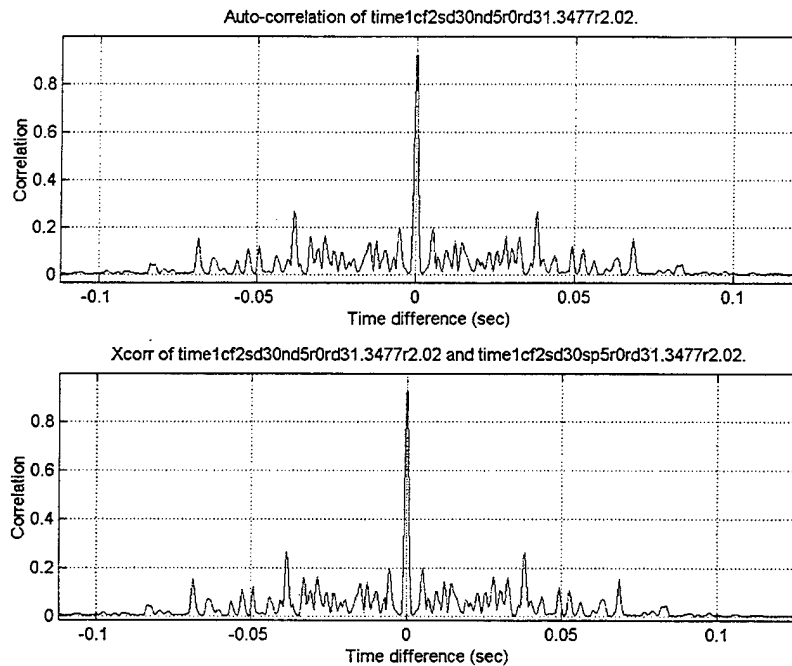


Figure 8: Correlation for a source depth of 30 m and a receiver depth of 30 m comparing source speed of 5 m/s with no roughness to that of no Doppler and no roughness.

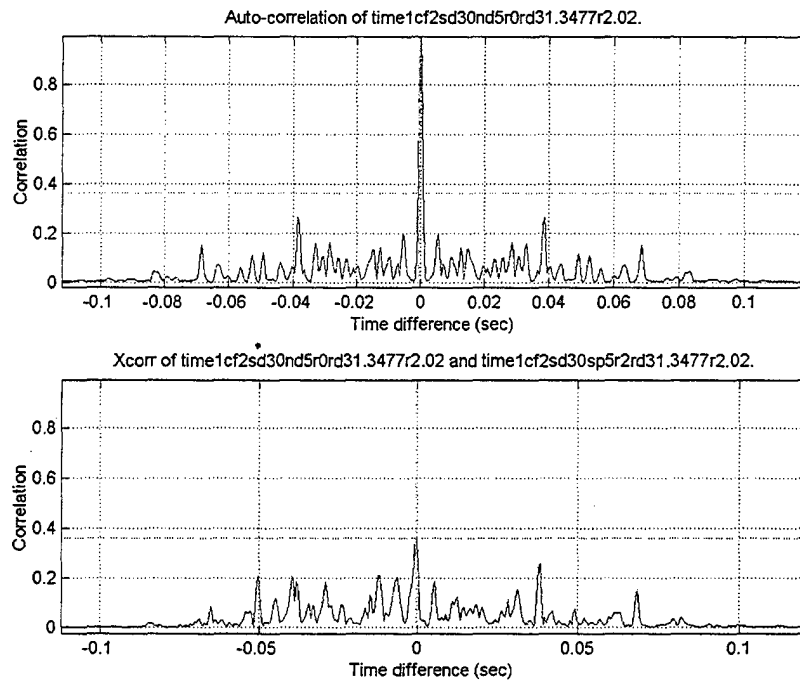


Figure 9: Correlation for a source depth of 30 m and a receiver depth of 30 m comparing source speed of 5 m/s with a roughness of 2 m to that of no Doppler and no roughness.

Taking the maximum amplitudes for each of the cross-correlations and plotting them as a function of receiver range provides some additional information. Figure 10 is a set of graphs for SVP 1 with a source depth of 30 m for the two cases with a roughness of 2 m.

Figures 10(a,b) demonstrate the decorrelation of the signal over various ranges. The correlation for the various conditions remains below 0.5 for all but a couple of ranges. This is the same for all of the source/receiver depths for SVP 2. Figures 10(c,d,e,f) start with a maximum correlation above .5 at short ranges (2 km) and decrease with range. Both Figures 10 and 11 demonstrate a higher correlation for source and receiver depths of 50 m and greater that remains high for all ranges studied. A relationship between center frequency and maximum correlation for ranges between 2 and 4 km is demonstrated in Figures 10(c, d) and 12(a, b). The increased correlation for

deeper source/receiver depths for SVP 1 is possibly due to the formation of a deep sound channel resulting in less bottom interaction. In general, Figures 10, 11, and 12 appear to have no apparent relationship between center frequency and the maximum correlation in the presence of bottom roughness.

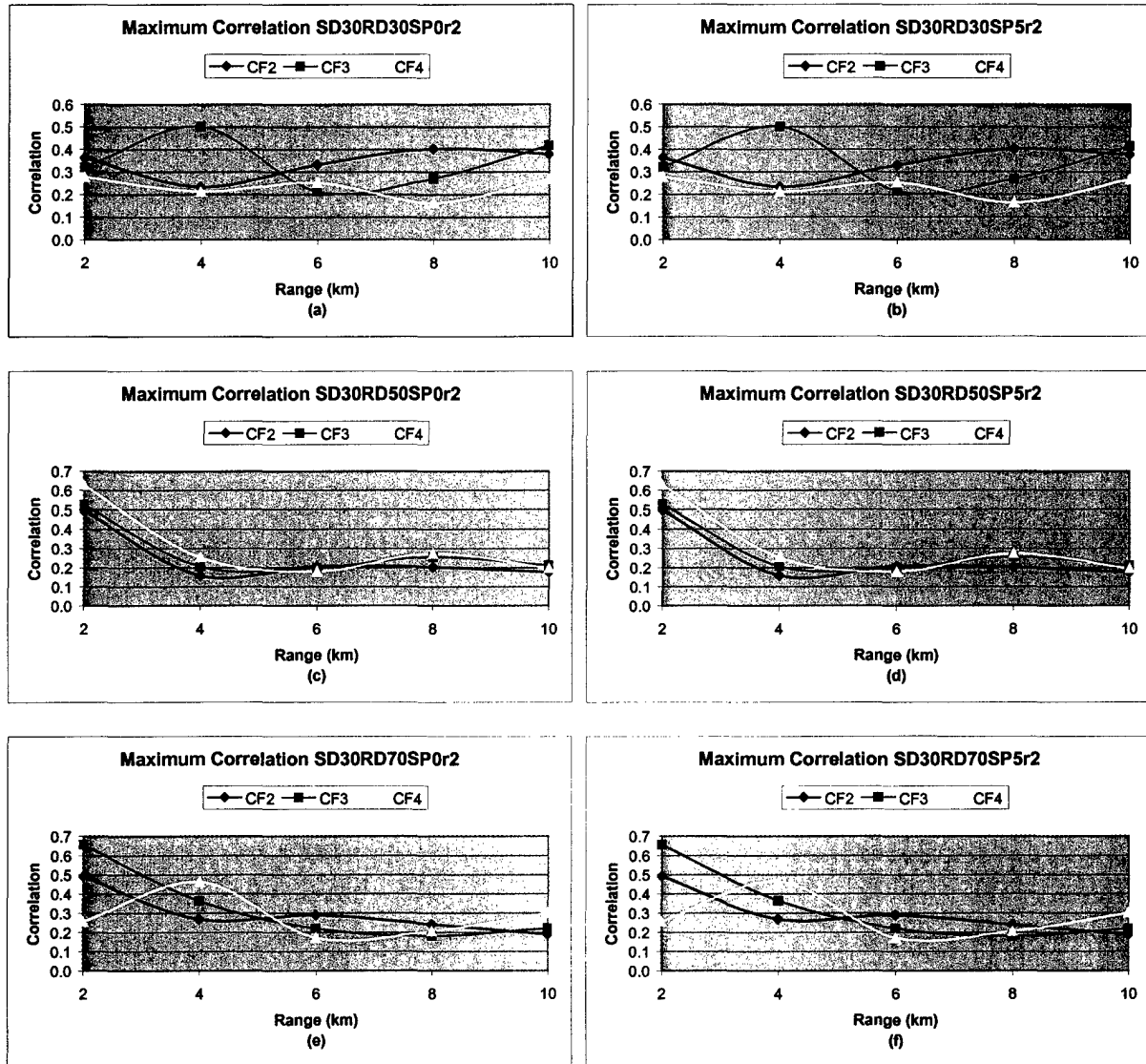


Figure 10: Maximum value of the cross-correlation for each center frequency with a roughness of 2 m and zero speed for (a, c, e) and a roughness of 2 m and speed of 5 m/s for (b, d, f). The data was calculated using SVP 1, a source depth of 30 m and receiver depths of (a, b) 30 m, (c, d) 50 m, and (e, f) 70 m.

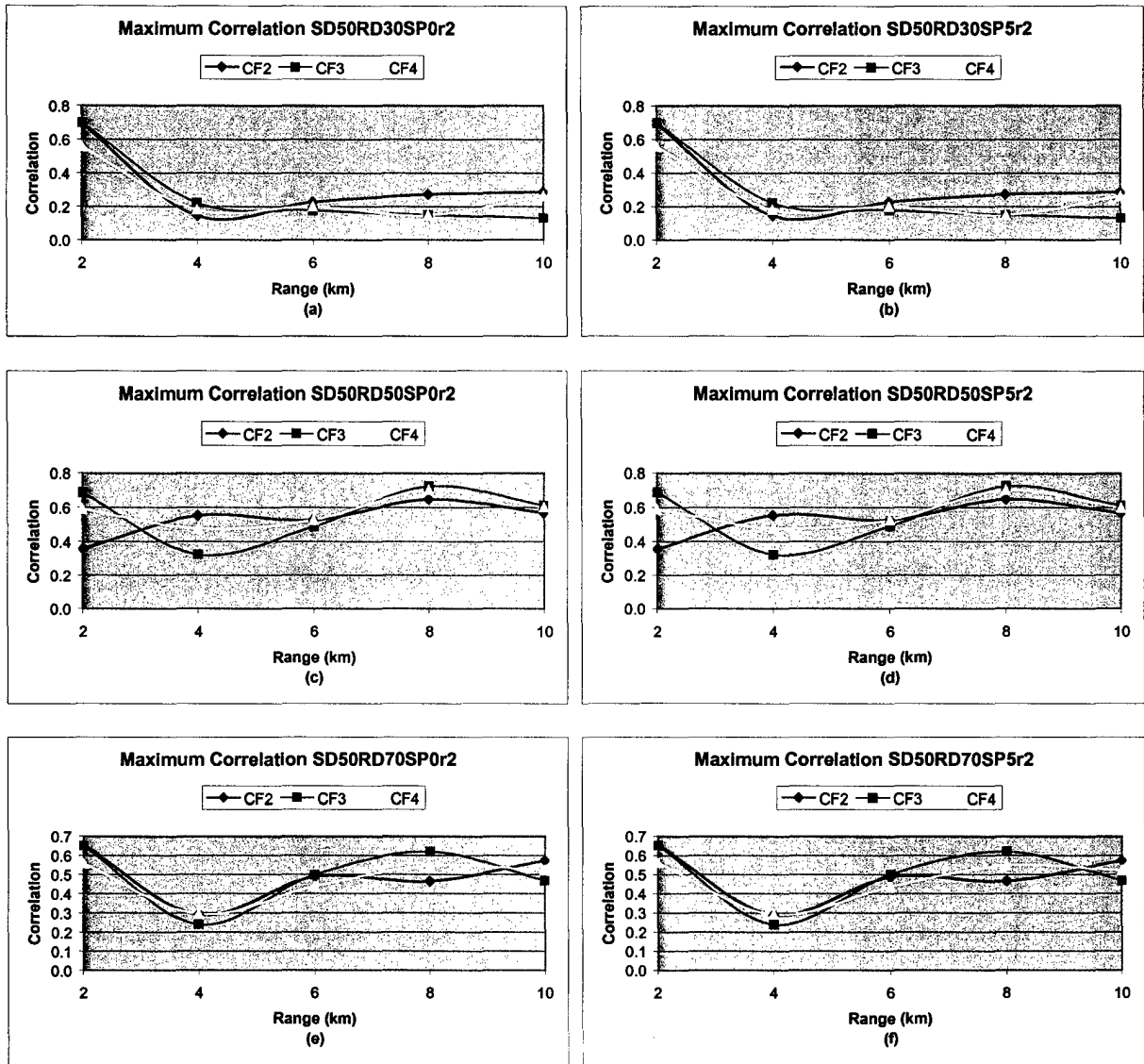


Figure 11: Maximum value of the cross-correlation for each center frequency with a roughness of 2 m and zero speed for (a, c, e) and a roughness of 2 m and speed of 5 m/s for (b, d, f). The data was calculated using SVP 1, a source depth of 50 m and receiver depths of (a, b) 30 m, (c, d) 50 m, and (e, f) 70 m.

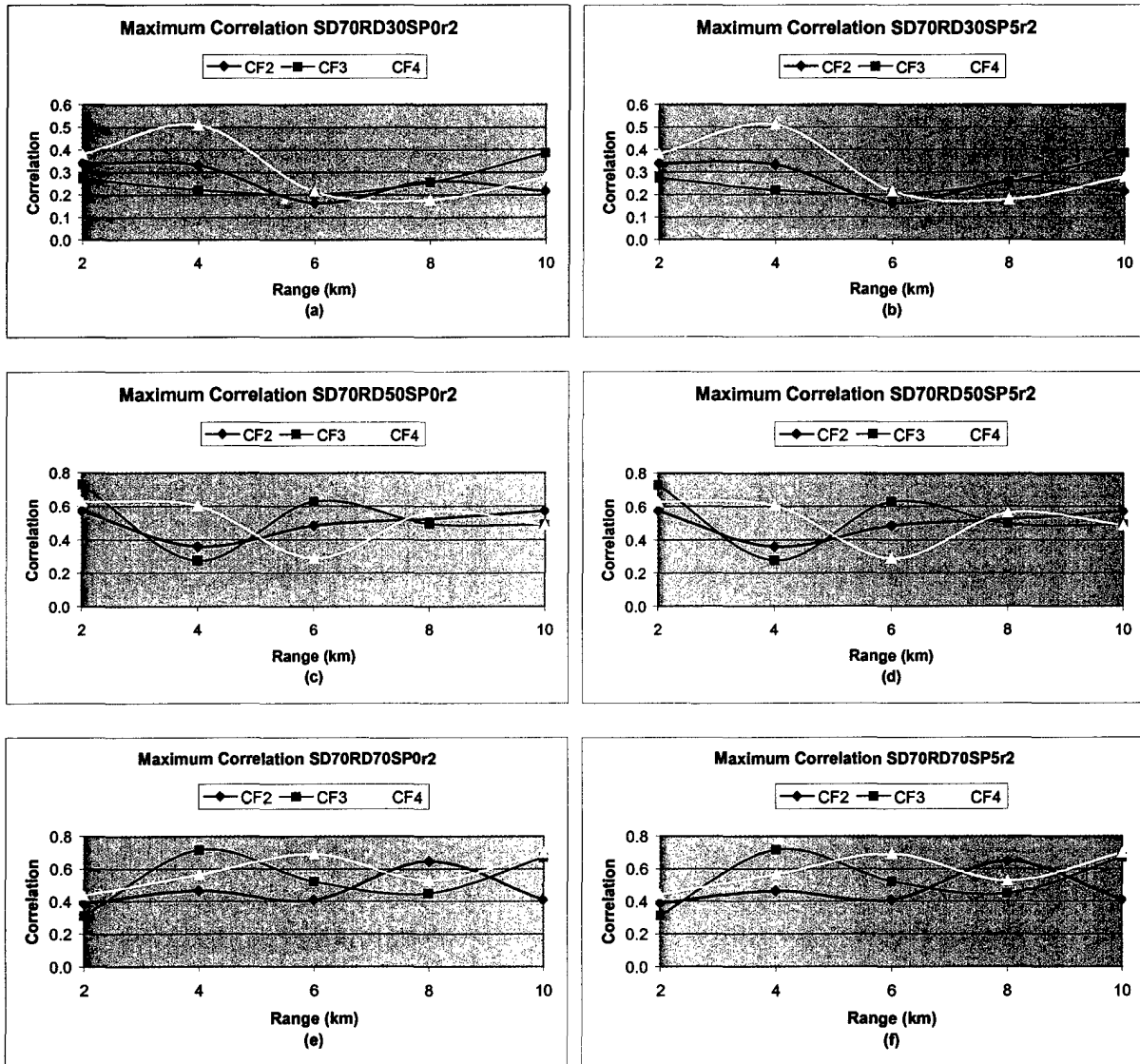


Figure 12: Maximum value of the cross-correlation for each center frequency with a roughness of 2 m and zero speed for (a, c, e) and a roughness of 2 m and speed of 5 m/s for (b, d, f). The data was calculated using SVP 1, a source depth of 70 m and receiver depths of (a, b) 30 m, (c, d) 50 m, and (e, f) 70 m.

However, when no roughness is included and Doppler alone is introduced, the cross-correlations do exhibit a frequency dependence. This is illustrated in Figure 13. It is representative of all of the combinations of SVP, source depth and receiver depth. In this case, there is a relationship between center frequency and maximum correlation. It is

observed that the lower center frequency has a higher cross-correlation value. It is a slight difference, but it was true for all cases studied. In general, all of these correlation values were very high, suggesting that Doppler effects due to source motion do not significantly degrade signal coherence.

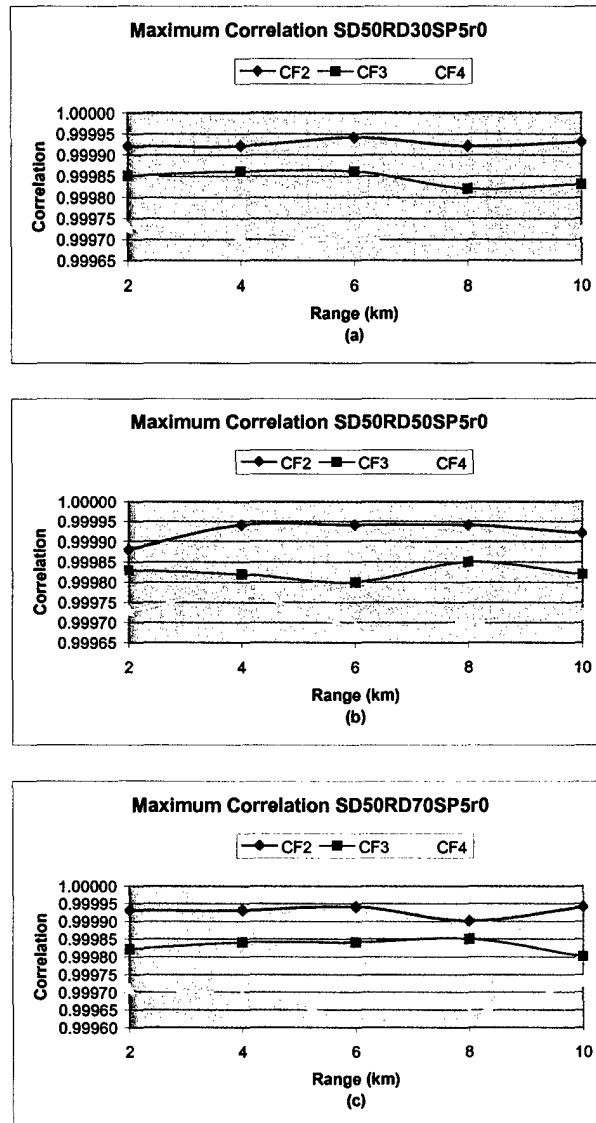


Figure 13: Maximum value of the cross-correlation for each center frequency with no roughness and a source speed of 5 m/s and for a receiver depth of (a) 30 m, (b) 50 m, and (c) 70 m for SVP 1 and a source depth of 50 m.

An abrupt change of 2 m rms bottom roughness is not very likely, but is good for analyzing effects of a changing interface. Another approach, however, would be to shift the bottom some distance while keeping the structure of the bottom roughness realization the same. This would mimic the effect of source displacement. To study this effect, a bottom shift of 6.75 m was inserted into the MMPE model. For this new study, the time domain signals (no bottom shift and 5 m/s of source motion, bottom shift and no source motion, and bottom shift and source motion of 5 m/s, all with rms bottom roughness of 2 m) were cross-correlated with a reference time signal computed with no source motion and a rms bottom roughness of 2 m before shifting the bottom. Time domain signals compared had center frequencies of 2 and 4 kHz and source and receiver depths of 50 m.

The results of the bottom shifting for SVP 1, Figures 14(a,c,e), were similar to the results obtained for the abrupt change of 2 m with no relationship between the maximum cross-correlation and the center frequency. Figures 14(b,d,f), on the other hand, show a relationship for SVP 2, where the higher frequencies are more decorrelated than the lower frequencies. One reason for the differences between the results of SVP 1 and 2 is again the presence of a sound channel in SVP 1 which causes the signal to have less bottom interaction. This is also evident in the maximum value of the correlations in SVP 1 (average 0.76 for 2 kHz) being higher than in SVP 2 (average 0.54 for 2 kHz).

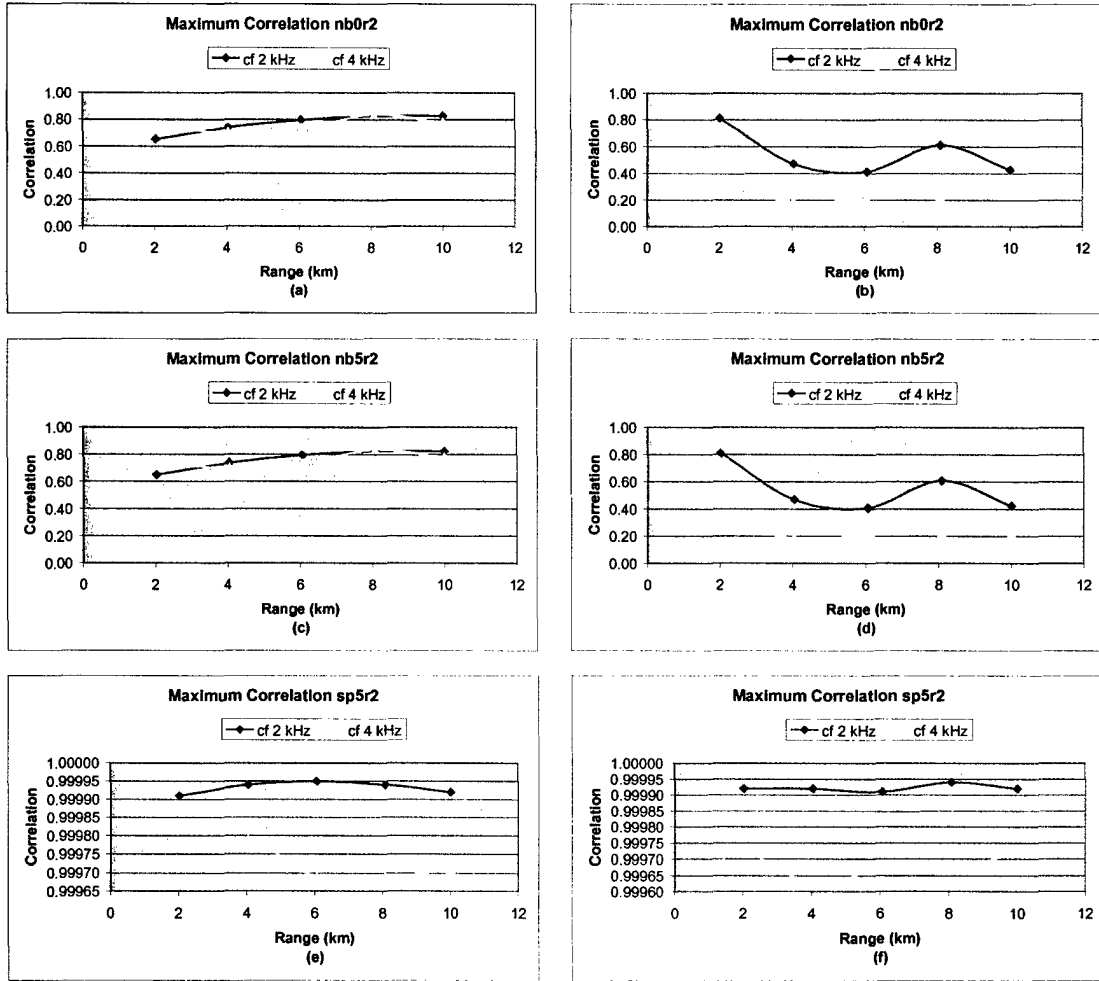


Figure 14: Maximum value of the cross-correlation for center frequency of 2 and 4 kHz with a rms bottom roughness of 2 m, a source and receiver depth of 30 m, and (a,b) bottom shift with no source speed, (c,d) bottom shift and source speed of 5 m/s, and (e,f) no bottom shift and source speed of 5 m/s for SVP 1 (a,c,e) and SVP 2 (b,d,f).

D. SPATIAL COHERENCE

The same center frequencies and bandwidths are considered for the spatial coherence as were used for the temporal coherence. At each range, the maximum amplitude of the cross-correlation was recorded and plotted in Figure 15.

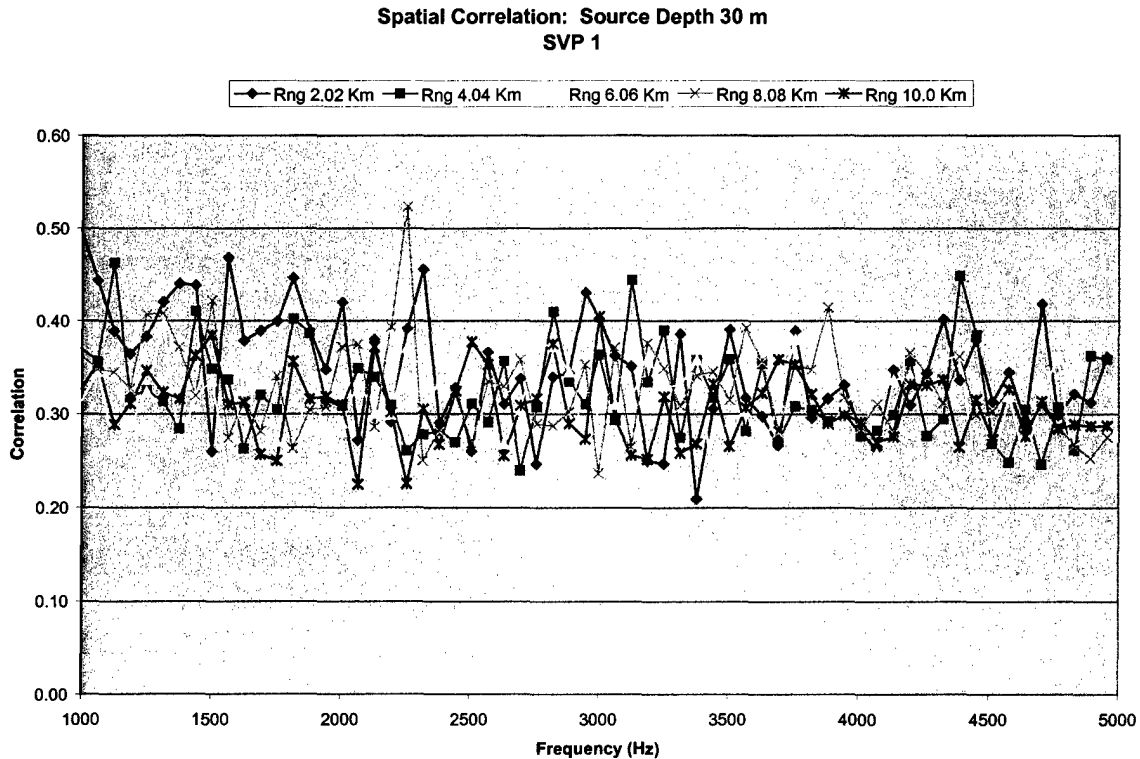


Figure 15: Plot of the maximum correlation for each frequency at each range for SVP 1 using no source speed and rms roughness of 2 m with source depth of 30 m.

Each of the source depths for both SVP's produced a similar plot. There is no appreciable difference between the cross-correlation and the frequency used. Furthermore, there isn't any difference between the no speed, 2 m rms roughness and the 5 m/s speed, 2 m rms roughness. The two maximum correlations in the signal were at most five percent apart.

Another way of looking at the data is to select five equally spaced frequencies and plot their peak correlations as a function of range. Figure 16 displays such plots for SVP 2. (The results for SVP 1 are similar to those for SVP 2.) The plots in Figures 16(a,c,e) show no relationship between frequency and maximum correlation. Again we see that the bottom roughness causes the signal to become more decorrelated and that the 5 m/s Doppler shift with no bottom roughness is highly correlated with the reference signal. Unlike the temporal correlation, however, there doesn't seem to be the same frequency relationship with the maximum correlation and center frequency.

Bottom shifting can also be used to examine spatial coherence as we did for temporal coherence with the same parameters. Both SVP's show a relationship between frequency and the maximum value of the cross-correlation with the lower frequencies being more correlated to the reference signal than at higher frequencies. The data for SVP 1 is presented in Figure 17 and SVP 2 is presented in Figure 18. There is a stronger relationship using SVP 2 than using SVP 1. This is most likely due to the sound channel in SVP 1.

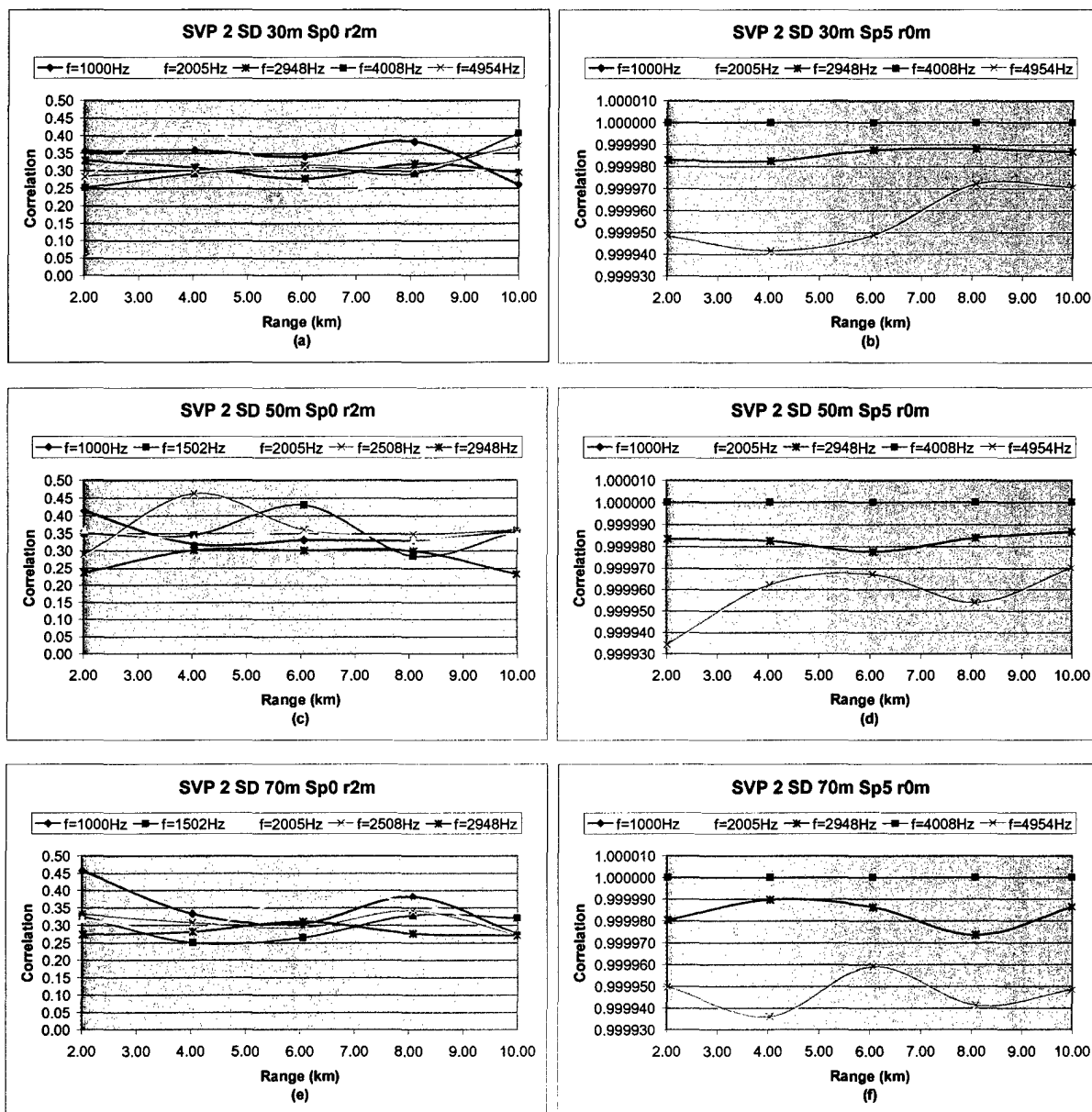


Figure 16: Plot of maximum correlation for source depths 30 m (a, b), 50 m (c, d), and 70 m (e, f) with (a, c), and (e) using no speed with roughness of 2 m and (b, d, f) using a speed of 5 m/s and roughness of zero.

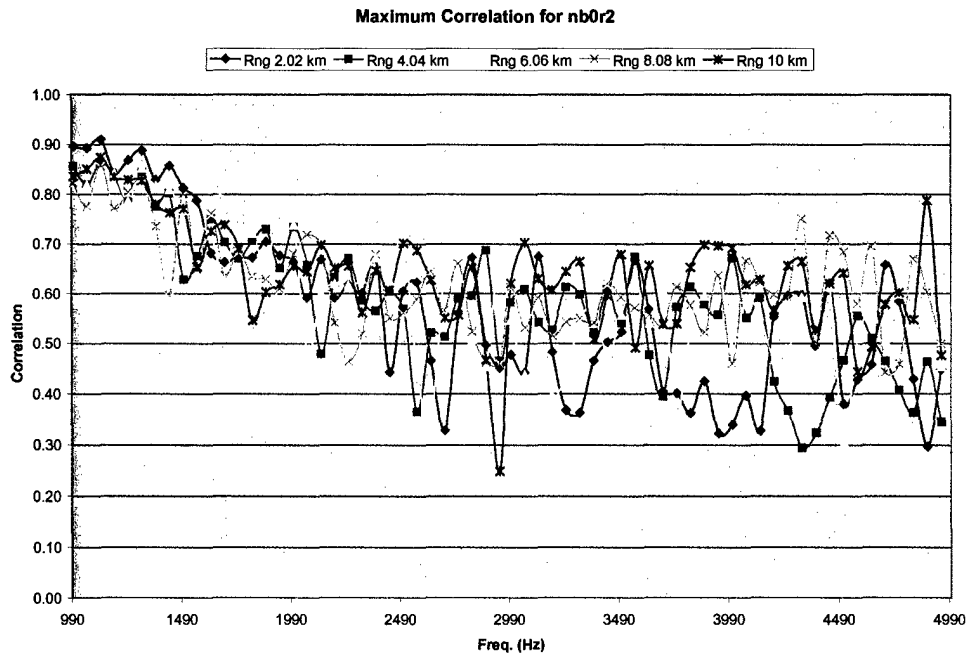


Figure 17: Plot of the maximum correlation for each frequency at each range for SVP 1 using the shifted bottom with no source speed and rms roughness of 2 m with source depth of 50 m

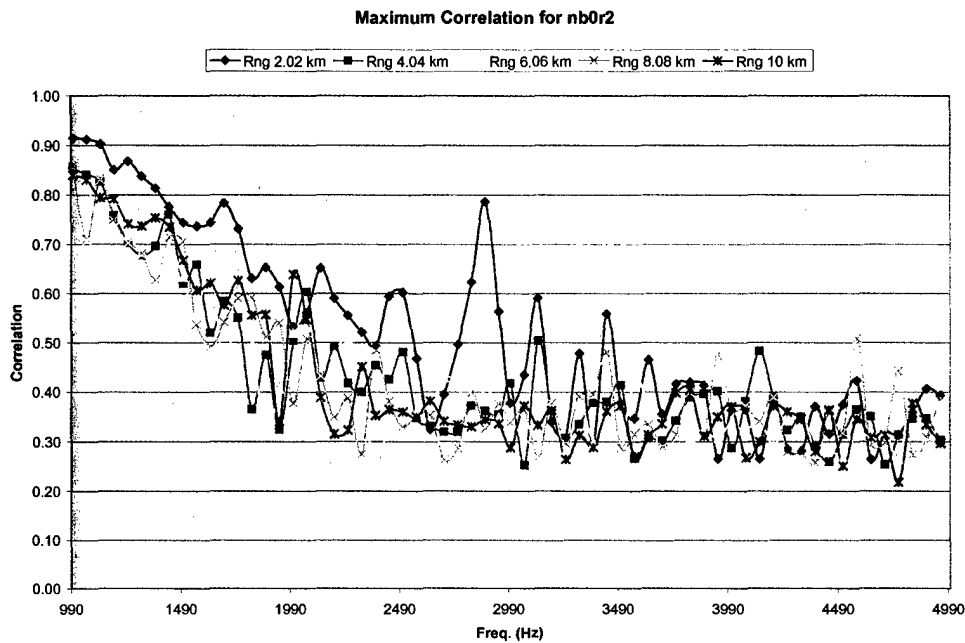


Figure 18: Plot of the maximum correlation for each frequency at each range for SVP 2 using the shifted bottom with no source speed and rms roughness of 2 m with source depth of 50 m.

IV. CONCLUSIONS

A. CONCLUSIONS

The focus of this thesis has been to find an optimum frequency band for an underwater acoustic communication channel. Only two SVP's were considered: one from the western Atlantic and one from the eastern Pacific. Source speeds were limited to 0 and 5 m/s, while the receiver speed was stationary, and various source/receiver configurations were considered. In addition, both a smooth bottom and a randomly rough bottom with rms value of 2 m were defined. Three methods of evaluation (transmission loss, temporal coherence, and spatial coherence) were employed.

The first MOE considered was transmission loss. TL was calculated for frequencies from 200 Hz to 5 kHz and ranges from 0 to 40 km. Relationships between TL and frequency are dependent on the bottom roughness and amount of signal interaction with the bottom. When either the bottom is smooth or the signal doesn't interact with the bottom very much, there does not appear to be any significant relationship. However, when there is strong interaction with the bottom and the bottom is rough (or has additional reflection loss mechanisms) it appears that higher frequencies experience greater transmission loss. The frequency producing the least TL appeared to be down near the lowest frequencies considered, roughly 200 Hz. Whether even lower frequencies would produce higher or lower TL values was not investigated. Over the frequency range of interest in this study, 1-5 kHz, there appeared to be approximately a 5-10 dB change in TL at a nominal range of about 10 km.

Next we considered the temporal coherence for source and receiver depths of 30, 50, and 70 m, rms bottom roughness of 0 and 2 m, and source speeds of 0 and 5 m/s. For a reference signal with no Doppler and a smooth bottom, the only correspondence between frequency and maximum correlation of the time signal was observed for a smooth bottom where lower frequencies exhibited high correlations. However, all of these correlation values were very high, indicating that the influence of Doppler alone does not degrade signal coherence.

Then the bottom was shifted by 6.75 m, maintaining the same 2 m rms bottom roughness. This simulated source displacement. Correlating a signal with this new "shifted" bottom and a reference of no source motion and 2 m rms bottom roughness, a relationship was recognized between center frequency and correlation. It was observed that the higher frequency cross-correlations were more decorrelated than the lower frequencies. For this source displacement, the signals were less than 80% correlated for frequencies above about 1500 Hz. This displacement then corresponds to approximately 7 wavelengths.

A similar analysis was performed to determine the spatial coherence. Varying rms bottom roughness between 0 and 2 m produced no relationship between center frequency and the maximum correlation. When the bottom was "shifted", the same relationship was discovered as in the temporal coherence case, that the higher frequency cross-correlations were more decorrelated.

Based on the relationships observed for transmission loss, temporal coherence, and spatial coherence, it appears that the optimization of the communications bandwidth is highly dependent on the characteristics of the environment. In this study, the dominant

influence on signal level and coherence appeared to be the introduction of roughness on the bottom interface. Source motion relative to this roughness (i.e., displacement) appeared to cause significant signal degradation at higher frequencies. However, Doppler effects due to source motion did not seem to appreciably influence signal coherence. Furthermore, the influence of the bottom roughness was clearly affected by the presence, or lack of, a sound channel. Specifically, if a sound channel existed which limited the amount of bottom interactions, then the source motion (Doppler or displacement) did not seem to significantly affect signal coherence. It is expected that similar conclusions would be obtained by introduction of a rough surface.

Given the conditions considered here, if the sound velocity profile generates significant bottom interactions, then the optimal frequency bandwidth appears to be the lowest possible, particularly at ranges beyond approximately 1 km. For weakly bottom interacting profiles, higher frequencies that can increase data transfer rates would be optimal. The limitations of such higher frequencies would predominantly be in TL, but even this did not exhibit appreciable frequency dependence for ducted propagation.

B. RECOMMENDATIONS FOR FURTHER RESEARCH

As with most studies, areas of research were left that require further investigation. One of these areas is a more detailed study of the affect of the shifting bottom (or source displacement). In this study, only a shift of 6.75 m was analyzed. Including multiple shift ranges and source/receiver depths would provide a better idea of how significant these effects are on the temporal and spatial coherences.

Another area of research would be to evaluate the effect of different bottom roughnesses and the influence of other bottom properties such as sheer or volume inhomogeneities. Further effort should also be made in determining the effects of environmental parameters not considered. These environmental parameters could include internal waves or rough surface interactions.

To complement the implementation of source motion, continued studies to include receiver motion could produce some insight into the correlation of the signal. In the temporal coherence section, it was noticed that higher frequencies were more decorrelated than lower frequencies in the presence of source motion. Despite being weak, receiver motion could intensify the decorrelation making it more significant.

As developers are trying to increase the data rates, a study to include both higher operating frequencies and larger bandwidths could be of use. Additionally, further studies should include ranges out to 60 to 80 km.. This information could lead to such information as optimal bin widths, power requirements, and detectable ranges.

LIST OF REFERENCES

Curtin, T. B. and Benson Jr., R. A. (1999). "ONR Program in Underwater Acoustic Communications," *Sea Technology*, Volume 40, Number 5, pp. 17-27.

Jensen, F. B. and Kuperman, W. A. (1983). "Optimum frequency of propagation in shallow water environments," *J. Acoust. Soc. Am.*, Volume 73, pp 813-818.

Jensen, F. B., Kuperman, W. A., Porter, M. B., Schmidt, H. (2000). *Computational Ocean Acoustics* (Springer-Verlag New York, Inc., 2000).

Kilfoyle, D. B. and Baggeroer, A. B. (2000). "The State of the Art in Underwater Acoustic Telemetry," *IEEE Journal of Oceanic Engineering*, Volume 25, Number 1, pp. 4-27.

Kilfoyle, D. B. and Baggeroer, A. B. (1999). "Research Directions in Underwater Acoustic Telemetry," *Sea Technology*, Volume 40, Number 5, pp. 10-15.

Kinsler, L. E., Frey, A. R., Coppens, A. B., Sanders, J. V. (2000). *Fundamentals of Acoustics* (John Wiley & Son, Inc., 2000).

Li, L. S. (2000). "Parabolic Equation Modeling of Bottom Interface and Volume Reverberation in Shallow Water," Master's Thesis, Naval Postgraduate School, Monterey, CA, September 2000.

Proakis, J. G. and Manolakis, D. G. (1996). *Digital Signal Processing, Principles, Algorithms, and Applications* (Prentice-Hall, Inc, 1996).

Smith, K. B. and Tappert, F. D. (1993). "UMPE: The University of Miami Parabolic Equation Model, Version 1.1," Marine Physical Laboratory Technical Memorandum 432, May 1993.

Smith, K. B. (2001a). "Convergence, stability, and variability of shallow water acoustic predictions using a split-step Fourier parabolic equation model," *J. Comp. Acoust.*, Volume 9, Number 1.

Smith, K. B. (2001b). "Computing the Influence of Doppler due to Source/Receiver Motion in Parabolic Equation Models," *J. Comp. Acoust.* (submitted 2001).

Stojanovic, M., Catipovic, J. A., and Proakis, J. G. (1993). "Adaptive multi-channel combining and equalization for underwater communications," *J. Acoust. Soc. AM.*, Volume 94, pp 1621-1631.

Thomson, D. J. and Chapman, N. R. (1983). "A wide-angle split-step algorithm for the parabolic equation," *J. Acoust. Soc. AM.*, Volume 74, pp 1848-1854.

INITIAL DISTRIBUTION LIST

1. Defense Technical Information Center 2
8725 John J. Kingman Road, Suite 0944
Ft. Belvoir, VA 22060-6218
2. Dudley Knox Library 2
Naval Postgraduate School
411 Dyer Road
Monterey, CA 93943-5101
3. Prof. K.B. Smith, Code PH/Sk..... 6
Department of Physics
Naval Postgraduate School
Monterey, CA 93943-5002
4. Prof. D. Brutzman, Code UW/Br 1
Department of Undersea Warfare
Naval Postgraduate School
Monterey, CA 93943
5. Dr. D. T. Nagle..... 2
Naval Undersea Warfare Center, Division Newport
Attn: D. Nagle (C8212)
1176 Howell St.
Newport, RI 02841
6. LT J.E. Houdeshell..... 2
363 B. Shark Blvd.
Groton, CT 06340